

Mitigating Chromatic Dispersion with Hybrid Optical Metasurfaces

Rajath Sawant, Purva Bhumkar, Alexander Y. Zhu, Peinan Ni, Federico Capasso,* and Patrice Genevet*

Metasurfaces control various properties of light via scattering across a large number of subwavelength-spaced nanostructures. Although metasurfaces appear to be ideal photonic platforms for realizing and designing miniaturized devices, their chromatic aberrations have hindered the large-scale deployment of this technology in numerous applications. Wavelength-dependent diffraction and resonant scattering effects usually limit their working operation wavelengths. In refractive optics, chromatic dispersion is a significant problem and is generally treated by cascading multiple lenses into achromatic doublets, triplets, and so on. Recently, broadband achromatic metalenses in the visible have been proposed to circumvent chromatic aberration but their throughput efficiency is still limited. Here, the dispersion of refractive components is corrected by leveraging the inherent dispersion of metasurfaces. Hybrid refractive-metasurface devices, with nondispersive refraction in the visible, are experimentally demonstrated. The dispersion of this hybrid component, characterized by using a Fourier plane imaging microscopy setup, is essentially achromatic over about 150 nm in the visible. Broadband focusing with composite plano-convex metasurface lenses is also proposed. These devices could find applications in numerous consumer optics, augmented reality components, and all applications including imaging for which monochromatic performance is not sufficient.

achromatic broadband response has even been reported by manipulating scalar properties of light^[3] or by utilizing structural dispersion of surface plasmon polaritons in metal–insulator–metal waveguides to compensate for metal dispersion.^[6] Various high-efficient components like polarizers,^[7,8] holograms,^[9,10] beam splitters^[11] have been already designed using metasurfaces. A recent report on gradient silicon metasurface device showed a beam deflector having 71% transmission efficiency and 95% diffraction efficiency, and operating at a specific wavelength of 532 nm.^[12] The dispersion of metasurfaces can be varied from positive to zero and even to a negative value in the infrared region.^[4,5] This control enables devices such as achromatic deflectors and lenses.^[5,13–17] The general method proposed to engineer a frequency-dependent phase profile $\phi(\vec{r}, \omega)$, thereby achieving arbitrary control of metalens dispersion over a continuous bandwidth, requires one to separately engineer the phase, group delay, and the group delay dispersion of each nanoelement forming the metasur-

face.^[13–15] This procedure is rather complex and requires multiple degrees of freedom in the nanostructures, and is generally performed by considering systematic parameter search at given frequencies. To operate over a certain bandwidth of interest, these constraints limit the size and the numerical aperture (NA)—or the slope of the local phase gradient—of the devices. In this contribution, we address the problem of chromatic dispersion of conventional refractive components by coupling refractive devices with metasurface phase elements to carefully balance the material dispersion over a broadband range of wavelengths. This approach is relatively simple and can easily be combined with various devices, including high numerical aperture lenses^[18] and various beam-shaping devices. The dispersionless property of geometric phase has been exploited in achieving achromatic broadband imaging by superoscillatory metasurfaces^[19] and to execute achromatic performance in catenary-based orbital angular momentum generators.^[20] In contrast to previous works that leverage the geometric and/or multimode phase property of nanoantennae to fully address the dispersive response of the metasurface alone,^[21] here we demonstrate achromaticity by combining conventional

The macroscopic size of conventional optical components based on refractive optics significantly limits the miniaturization of optical systems. In addition, the dispersive response of bulk materials introduces strong chromatic aberrations. Metasurfaces, ultrathin devices composed of subwavelength array resonators can effectively overcome this problem.^[1–5] Low-efficiency

R. Sawant, P. Bhumkar, Dr. P. Ni, Dr. P. Genevet

CNRS

CRHEA

Université Côte d'Azur, rue Bernard Gregory

Sophia Antipolis

06560, Valbonne, France

E-mail: pg@crhea.cnrs.fr


A. Y. Zhu, Prof. F. Capasso

John A. Paulson School of Engineering and Applied Sciences

Harvard University

Cambridge, MA 02138, USA

E-mail: capasso@seas.harvard.edu

 The ORCID identification number(s) for the author(s) of this article can be found under <https://doi.org/10.1002/adma.201805555>.

DOI: 10.1002/adma.201805555

dispersive devices with diffractive phase gradient metasurfaces. Calculations, done in the context of achieving broadband achromatic focusing across the entire visible, have shown that, to suppress chromatic aberrations, one needs to address both group delay $\left(\frac{\partial\phi}{\partial\omega}\right)$ and group delay dispersion $\left(\frac{\partial^2\phi}{\partial\omega^2}\right)$.^[13]

This has been realized by considering the dispersive nature of the resonances of nanostructures forming the metasurfaces. Such a level of refinement, which is beyond the scope of the work discussed here, is necessary to obtain fully achromatic devices. In ref. [22] the authors' simulations also showed that the dispersive properties of a single metasurface can be engineered to compensate the glass dispersion of a plano-convex refractive lens, leading to achromatic focusing across the visible spectrum. Inspired by these works, we show that the diffractive properties of simple phase gradient metasurfaces are already sufficient to mitigate the dispersive behavior of one of the most common dispersive components, i.e., a prism. The latter was historically used by Sir Newton to separate light into its constituent spectral colors. Coupling it with phase gradient metasurfaces, we theoretically propose and experimentally show identical refraction angle for all colors within a certain range of wavelength around the designed frequency. We discuss extension of this method to other components, and as an example we realize high transmitting weakly dispersive focusing of light over a large range of frequencies.

For the sake of simplicity, we start by considering a glass prism refractive material working in the 500–800 nm wavelength range, where the refractive index can be Taylor-expanded around λ_0 (700 nm) as $n(\lambda) = A - \frac{2B}{\lambda_0^3}\lambda + \frac{3B}{\lambda_0^5}$ where A and B are Cauchy's coefficients of the prism material. In this wavelength range, the dispersion is weak and can be approximated by just a linear function. This limit of weak dispersion simplifies our analysis to the case of linearly phase gradient metasurfaces. In principle, one could also extend this approach to more complex nonmonotonic dispersion. Generalized laws of refraction can thereby be used to calculate the angle of deflection for the prism–metasurface doublet^[23] (see Section S1 in the Supporting Information). After a few algebraic simplifications, we obtain the relation for the phase gradient that compensates linear prism dispersion given by

$$\frac{d\phi'}{dx'} = \frac{2\pi B}{\lambda_0^3} \quad (1)$$

This expression is valid for a given incident angle and a prism with a given apex angle, meaning that new sort of aberrations would be present for any other incident angle. As discussed in Section S1 of the Supporting Information, Equation (S25) shows that a change in incident angle θ_i requires us to adjust the phase gradient accordingly. However, it should be ensured that the incident angle is less than the critical angle to prevent total internal reflection. For the given prism geometry it was found out that the incident angle can take any arbitrary value from -90° to 16° after which the refracted ray gets internally reflected.

As discussed in details in the Supporting Information, in the case of normal dispersion, the deflection increases with the wavelength toward the base of the prism. Compensation is achieved by adding a metasurface at the exit interface that can introduce a momentum in the opposite direction, i.e. toward the apex of the prism. In this configuration, the experimental results, presented in Figure 1c–e, comprise two intensity dispersion curves representing the zero-order transmission (lower line) and corrected case (first-order diffraction of the dispersive device with the metasurface). It is important to note that since the metasurface adds an additional transverse momentum to the refracted light, the achromatic refraction occurs at an angle of 49.59° which is different from the normal refraction at an angle of 49.22° for the central wavelength. To simultaneously observe and compare the dispersive properties of the rectified first order with respect to the zero order, we enlarged the spot size of the incident light to be larger than metasurface, i.e., part of the light is interacting with metasurface and part of the light is normally refracted by the prism only.

As evidenced by Figure 1, because of the small dispersion of the refractive material considered in the wavelength range of interest, the k -space spectra of the bare prism (lower intensity line in Figure 1c–e) as a function of wavelength, shows only small angle changes. Such a regime of small dispersion is required to validate our simple Taylor expansion calculations, but one can further expand this method to regime with higher dispersion. In our case, the momentum to be introduced by the metasurface has to be relatively small (4×10^{-5} rad nm⁻¹). As a result, we expect the dispersion curves of normally and anomalously refracted signals to be very close to each other, as shown in Figure 1c–e. Appropriate information is obtained by maximizing the pixel-to-pixel k -space resolution. This is experimentally performed by using a low-NA microscope objective (4 \times) and by collecting the refracted beam along the optical axis of the microscope objective, i.e., by rotating the sample and incident light accordingly such that both refracted beams exit almost collinear with the microscope objective, within its collection angles. To correctly extract information from these measurements, we calculate the slope and the associated error of the dispersion curves, with and without the metasurface, as discussed in details in Section S4 in the Supporting Information. The results, presented in Table 1, show that metasurfaces can effectively compensate the dispersion in the range 600–800 nm. Beside the small deviations, which we attribute to the linear approximation of the refractive index, the fabrication imperfections and small misalignment in the optical setup, our simple example shows that metasurface and material dispersions could be combined to achieve essentially achromatic refraction in a given range of frequency. This approach could be extended to more complex

Table 1. The deflection angle results, which confirm that the metasurface helps to rectify the dispersion of the prism.

Wavelength [nm]	Prism k_y/k_0 per nm ($\times 10^{-5}$)	Prism+metasurface k_y/k_0 per nm ($\times 10^{-5}$)	Percentage of compensation (mean value)
540–600	-4.2 ± 0.1	-2.0 ± 0.5	52%
600–700	-2.8 ± 0.1	-0.5 ± 0.9	82%
700–800	-1.4 ± 0.1	0.2 ± 0.6	114%

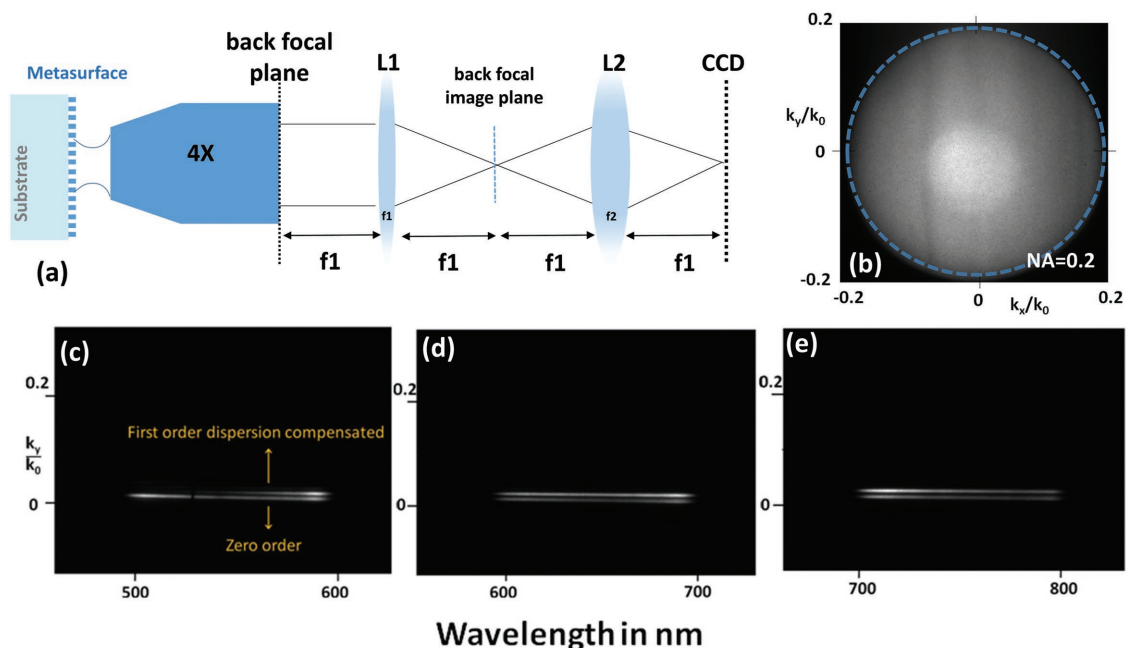


Figure 1. *k*-space imaging of metasurfaces. a) Setup for *k*-space imaging of the transmitted light through a metasurface. Light refracted through the metasurface is collected with a relatively low numerical aperture objective (NA = 0.2). The spatial Fourier transform of light in the front focal plane is imaged using a 4*f* relay from the back focal plane of the objective onto the entrance aperture of a spectrometer coupled to an intensified CCD camera. b) To calibrate the image obtained with our experimental setup, we imaged the *k*-space reflectivity of a bright light source on a silicon substrate at the zero diffraction order of the spectrometer grating. This image shows intensity distribution that covers the entire NA of the microscope objective, in the range of $-0.2 < \frac{k_y}{k_0} < 0.2$. c–e) Both normal refraction and dispersion compensated refraction for three different frequency range ranging from: 1) 500–600 nm, 2) 600–700 nm to 3) 700–800 nm. The *y*-axis of the *k*-space image is normalized to *k*₀. The result of this experiment is analyzed by looking at the slopes of the dispersed signal.

geometries and in particular to compensate for the chromatic dispersion of a conventional plano-convex lens.

In the following, we propose a method to mitigate the focal length shift of a plano-convex lens over a given range of wavelength by considering a radially varying phase gradient metasurface patterned along the planar surface of the lens. Note that the compensation effect presented in this section is essentially caused by the diffracting properties of the metasurfaces, which differs from the antenna dispersion compensation approach previously reported in the Supporting Information of ref. [22], i.e., we are considering the refraction through dispersive lens, assuming it is working in the regime of linear dispersion approximation. Compared to the results on the prism, we are replacing the uniform phase gradient metasurfaces with radially varying phase delay interfaces to mitigate the effect of refraction. After some algebraic calculations detailed in Section S6 in the Supporting Information, the expression for the radially varying phase gradient gives

$$\frac{d\phi}{dr} = \frac{4\pi B}{\lambda_0^3} \frac{r}{R} \quad (2)$$

In this calculation, we consider on axis parallel rays that are impinging upon the curved interface. “*R*” is the radius of curvature of the lens and “*r*” is the height of the ray from the optical axis. After deriving this expression, we implemented this metasurface in a ray-tracing Matlab code (Figure S5.2, Supporting Information), and extracted the focusing properties of our lens

system as a function of the incident wavelength. The results are presented in **Figure 2**.

The dispersion compensation is as high as ≈94% in the range of 600–800 nm for all “*r*” s. Note that although strong monochromatic aberrations are still present, one could extend this idea of metasurface compensator to address monochromatic aberration, as discussed in few papers already.^[24,25] While working in the infrared region, recent results showed the usage of metasurfaces for dispersion engineering with high average efficiency of 60% operating in the bandwidth 8–1.2 μm by custom-tailoring multiresonances.^[26]

We have successfully mitigated the dispersion of refractive optical components using a metasurface. Our method consists of combining a simple dispersive refractive component, a prism, with a linear phase gradient broadband metasurface working in the visible region from 500 to 800 nm. The achromatic behavior is observed in the range of 600–700 nm. Instead of designing complex metasurfaces that involve the control of the dispersive properties of the antenna resonance, we utilize the intrinsic dispersion of the phase gradient metasurface as a parameter to adjust the dispersive properties of the refractive object. In contrast to binary optics used to design hybrid diffractive/refractive components, the metasurface approach enables fabrication of phased elements with an arbitrary number of phase elements while requiring only a single step of lithography. We believe that hybrid metasurface/refractive devices, as proposed in this manuscript, could challenge the performances of binary optics

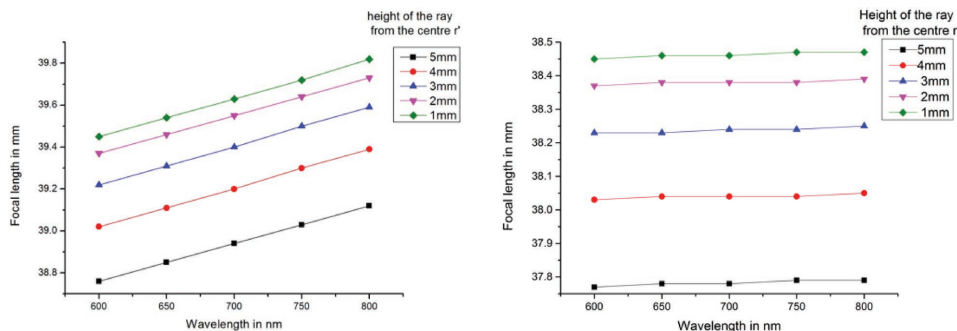


Figure 2. Ray-tracing analysis showing: a) dispersion/shift of the focal length for a plano-convex lens as a function of the wavelength. The different curves are given for gradually increasing off-axis ray, indicating both monochromatic and chromatic aberrations. The units on both axes are in mm. b) Same as in (a) but with chromatic aberration correction after introducing the metasurface.

designs. Fourier plane imaging plays a crucial role in this study, enabling accurate measurements of even small amounts of dispersion. Near dispersionless conditions are achieved with slight deviations due experimental errors. We extend this study to the design of a metasurface plano-convex lens. This technique is simple and can be very useful in addressing the problem of chromatic dispersion in multilayer/cascaded optical systems.

We are also expecting the development of new achromatic and aberration free devices by combining freeform optical components with conformal metadevices.^[27]

Experimental Section

The implementation of the metasurfaces with constant phase gradient satisfying Equation (1) was realized using TiO_2 phased array nanopillars

designed at 700 nm, i.e., the central wavelength around which the material refractive index was Taylor-expanded; see **Figure 3a**. TiO_2 nanopillars of diameters varying from 100 to 300 nm were fabricated on a glass substrate using electron beam lithography (EBL) technique and atomic layer deposition (ALD), as discussed previously in the literature.^[28] The phase shift imparted by each element as a function of its diameter is shown in the phase map (Figure 3b). Considering an incident circularly polarized light, Pancharatnam–Berry phase metasurfaces, such as those made of rectangular nanopillars or any structural birefringent nanostructures, could also give identical results.

The transmission map also indicated that the transmission remained very high for the range of wavelength considered in this study. This is because the nanopillars were behaving as truncated waveguides in this parameter regime, and were free from resonant effects.^[11] Note that dispersive response of these structures could be further engineered as well to improve the design of the hybrid components and to generalize the study into other wavelength regimes where material dispersion is

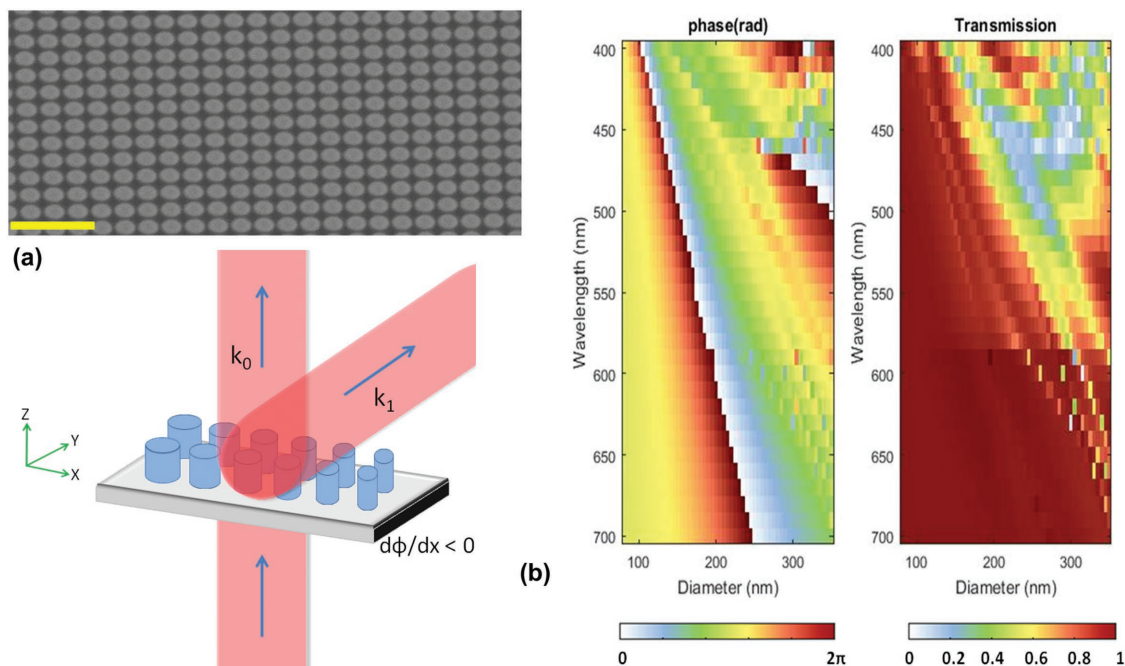


Figure 3. a) SEM image of TiO_2 nanopillars. Scale bar: 1 μm . The schematic in the bottom represents the zero- and first-order transmission of a phase gradient metasurface. b) Phase and transmission map of TiO_2 nanopillars computed using finite difference time domain simulation as a function of the incident wavelength and the nanopillar diameters. The simulations are performed considering in-plane periodic boundary conditions with a period of around 285 nm and perfect absorbing conditions on the top and the bottom of the simulation area.

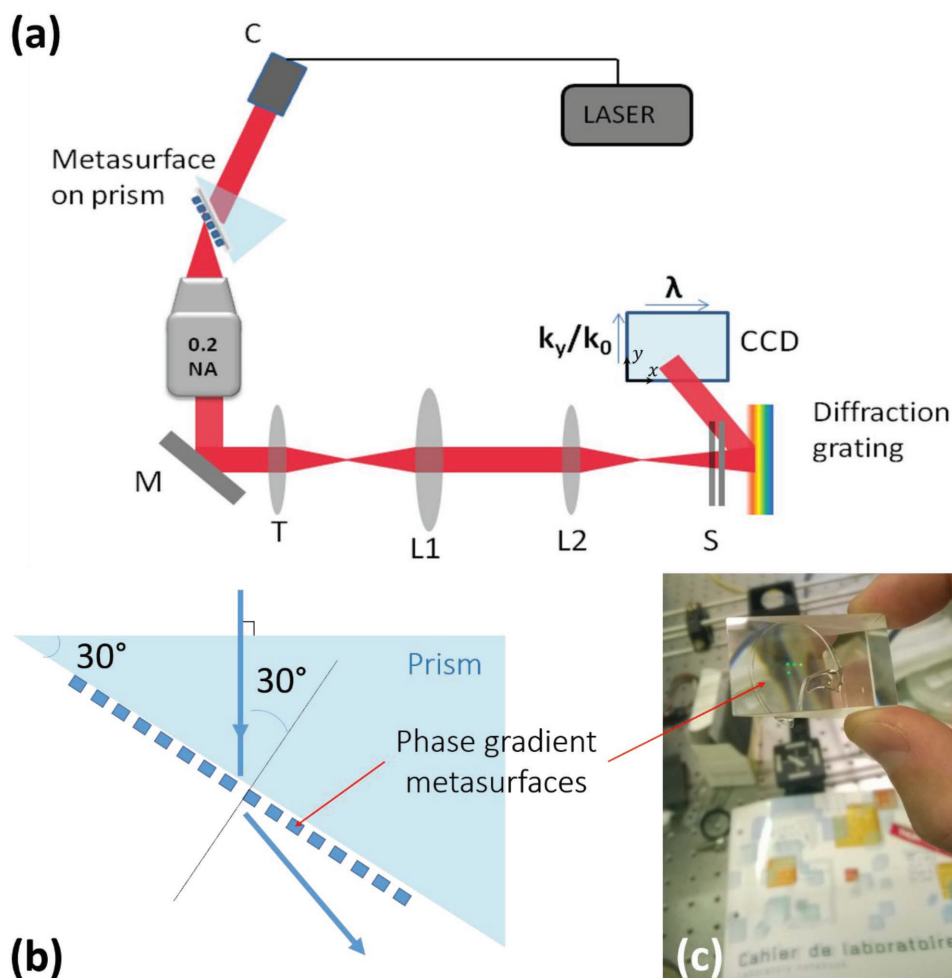


Figure 4. a) k -space imaging and spectroscopy setup for measuring the dispersion of the optical components: a supercontinuum laser NKT photonics laser coupled to a spectral filter is used as a source for the experiment. C: collimator, M: mirror, T: tube lens in the microscope setup, L1: achromatic convex lens of focal length $f_1 = 10$ cm, L2: achromatic convex lens of focal length $f_2 = 5$ cm, S: slit of the spectrometer. A microscope objective of 4 \times , 0.2 NA is used for imaging Fourier plane imaging. b) Schematic of the achromatic system. The light is normally incident at the input face of a refractive prism. At the output facet, in the absence of metacompensator, the wavelength-dependent refractive index of the prism should disperse the transmitted field accordingly to the conventional Snell laws. With the metasurface, the wavelength dispersion of the linear phase gradient, chosen with opposite dispersion compared to normal dispersion of refractive material, mitigates the dispersive effect of the prism. c) Picture of the experimentally realized achromatic optical component. The metasurface is assembled at the output facet of the prism using a thin layer of index-matching oil having sensibly the same properties of the glass prism.

typically nonlinear, but this level of refinement is beyond the scope here (Figure 4).

The dispersion was measured using a homemade k -space microscope. This system works by relaying the Fourier plane image of the objective lens to the entrance slit of an Andor Shamrock 500i spectrograph (500 mm focal distance), which was in turn coupled to an intensified iStar CCD camera using 4 f configuration of lenses.^[29–31] The 2D intensity map measured after spectrally dispersing the incident k -space image contained both spectral information (along the x dimension) and transverse k_y momentum information. Calibration of this experimental setup (Figure 1b) was performed by imaging the reflectivity of a substrate opening the spectrometer entrance slit and imaging the k -space, bringing the spectrometer diffraction grating to the zero order. The high intensity limits as denoted by the blue dashed circle giving $\left(\frac{k_x}{k_0}, \frac{k_y}{k_0} = |0.2|\right)$, occupy around 550 pixels on the CCD.

Since the NA of the objective is relatively small (0.2 NA), i.e., small angles were considered, and therefore $\sin\theta \approx \theta$ approximation was

made to consider that k_y/k_0 increased linearly from -0.2 to 0.2 . With this approximation, each pixel corresponded to a k_y/k_0 value of 7.3×10^{-4} units. To validate the accuracy of our experimental setup, the k -space spectra representing the dispersion of prism and metasurface were recorded separately; see Section S3 in the Supporting Information. For these two cases, dispersions with opposite slopes were observed, as expected from the opposite sign of dispersion properties of each component. The dispersion of this prism was measured and compared to known values for the material (BK7); see Section S3 in the Supporting Information. The transverse k -space (k_y) normalization of the Fourier plane image was determined by measuring the k_y^{\min} and k_y^{\max} of the objective lens used in this experiment. Further details are given in Section S3 of the Supporting Information. The slope of k_y versus λ is directly related to the linear dispersion of the light entering the microscope objective. With this measurement setup, achromatic dispersion was represented by an intensity line with vanishing slope, indicating no variation of the transverse k -vector as a function of the wavelength. The excitation of the prism–metasurface

system was performed using a collimated supercontinuum broadband laser coupled to a spectral filter to select 100 nm bandwidth around the targeted wavelength. The beam was directed to the metasurface after entering the prism at normal incidence from the input facet. This way, the incident angle at the exit facet was equal to the apex angle of 30°. The size of the beam spot, about 1 mm in diameter, impinges on the metasurface with a size sufficiently large to cover the entire metasurface. It was chosen to capture both normal and achromatic refraction in the same k -space image for direct comparison. By doing so, the dispersive properties for both first-order diffracted field (compensated refraction) and the zero-order (uncompensated) can be observed simultaneously on the CCD camera. The results of k -space experimental spectra are discussed in Figure 1c–e.

Supporting Information

Supporting Information is available from the Wiley Online Library or from the author.

Acknowledgements

R.S. and P.B. contributed equally to this work. This project was received funding from the European Research Council (ERC) under the European Union's Horizon 2020 research and innovation programme (Grant Agreement No. 639109) and from the Air Force Office of Scientific Research (Grants # FA9550-14-1-0389 and FA9550-16-1-0156).

Conflict of Interest

The authors declare no conflict of interest.

Keywords

dispersion, hybrid optics, metasurfaces, nanophotonics

Received: August 26, 2018

Revised: October 5, 2018

Published online: November 23, 2018

- [1] F. Aieta, M. A. Kats, P. Genevet, F. Capasso, *Science* **2015**, *347*, 1342.
- [2] B. Wang, F. Dong, Q. T. Li, D. Yang, C. Sun, J. Chen, Z. Song, L. Xu, W. Chu, Y. F. Xiao, Q. Gong, Y. Li, *Nano Lett.* **2016**, *16*, 5235.
- [3] P. Wang, N. Mohammad, R. Menon, *Sci. Rep.* **2016**, *6*, 21545.
- [4] E. Arbabi, A. Arbabi, S. M. Kamali, Y. Horie, A. Faraon, *Optica* **2017**, *4*, 625.
- [5] M. Khorasaninejad, Z. Shi, A. Y. Zhu, W. T. Chen, V. Sanjeev, A. Zaidi, F. Capasso, *Nano Lett.* **2017**, *17*, 1819.
- [6] Y. Li, X. Li, M. Pu, Z. Zhao, X. Ma, Y. Wang, X. Luo, *Sci. Rep.* **2016**, *6*, 19885.
- [7] B. X. Wang, C. Y. Zhao, Y. H. Kan, T. C. Huang, *Opt. Express* **2017**, *25*, 18760.
- [8] H. Kurosawa, B. Choi, Y. Sugimoto, M. Iwanaga, *Opt. Express* **2017**, *25*, 4446.
- [9] P. Genevet, F. Capasso, *Rep. Prog. Phys.* **2015**, *78*, 024401.
- [10] Z. L. Deng, G. Li, *Mater. Today Phys.* **2017**, *3*, 16.
- [11] D. Zhang, M. Ren, W. Wu, N. Gao, X. Yu, W. Cai, X. Zhang, J. Xu, *Opt. Lett.* **2018**, *43*, 267.
- [12] Z. Zhou, J. Li, R. Su, B. Yao, H. Fang, K. Li, L. Zhou, J. Liu, D. Stellinga, C. P. Reardon, T. F. Krauss, X. Wang, *ACS Photonics* **2017**, *4*, 544.
- [13] W. T. Chen, A. Y. Zhu, V. Sanjeev, M. Khorasaninejad, Z. Shi, E. Lee, F. Capasso, *Nat. Nanotechnol.* **2018**, *13*, 220.
- [14] S. Wang, P. C. Wu, V. C. Su, Y. C. Lai, C. H. Chu, J. W. Chen, S. H. Lu, J. Chen, B. Xu, C. H. Kuan, T. Li, S. Zhu, D. P. Tsai, *Nat. Commun.* **2017**, *8*, 187.
- [15] S. Wang, P. C. Wu, V. C. Su, Y. C. Lai, M. K. Chen, H. Y. Kuo, B. H. Chen, Y. H. Chen, T. T. Huang, J. H. Wang, R. M. Lin, C. H. Kuan, T. Li, Z. Wang, S. Zhu, D. P. Tsai, *Nat. Nanotechnol.* **2018**, *13*, 227.
- [16] E. Arbabi, A. Arbabi, S. M. Kamali, Y. Horie, A. Faraon, *Optica* **2016**, *3*, 628.
- [17] O. Avayu, E. Almeida, Y. Prior, T. Ellenbogen, *Nat. Commun.* **2017**, *8*, 14992.
- [18] R. Paniagua, Y. F. Yu, E. Khaidarov, S. Choi, V. Leong, R. M. Bakker, X. Liang, Y. H. Fu, V. Valuckas, L. A. Krivitsky, A. I. Kuznetsov, *Nano Lett.* **2018**, *18*, 2124.
- [19] Z. Li, T. Zhang, Y. Wang, W. Kong, J. Zhang, Y. Huang, C. Wang, X. Li, M. Pu, X. Luo, *Laser Photonics Rev.* **2018**, *12*, 1800064.
- [20] M. Pu, X. Li, X. Ma, Y. Wang, Z. Zhao, C. Wang, C. Hu, P. Gao, C. Huang, H. Ren, X. Li, F. Qin, J. Yang, M. Gu, M. Hong, X. Luo, *Sci. Adv.* **2015**, *1*, e1500396.
- [21] M. Khorasaninejad, W. T. Chen, R. C. Delvin, J. Oh, A. Y. Zhu, F. Capasso, *Science* **2016**, *352*, 1190.
- [22] W. T. Chen, A. Y. Zhu, V. Sanjeev, M. Khorasaninejad, Z. Shi, E. Lee, F. Capasso, *Nat. Nanotechnol.* **2018**, *13*, 220.
- [23] N. Yu, P. Genevet, M. A. Kats, F. Aieta, J. P. Tetienne, F. Capasso, Z. Gaburro, *Science* **2011**, *334*, 333.
- [24] A. Arbabi, E. Arbabi, A. M. Kamali, Y. Horie, S. Han, A. Faraon, *Nat. Commun.* **2016**, *7*, 13682.
- [25] F. Aieta, P. Genevet, M. A. Kats, F. Capasso, *Opt. Express* **2013**, *21*, 31530.
- [26] F. Zhang, M. Zhang, J. Cai, Y. Ou, H. Yu, *Appl. Phys. Express* **2018**, *11*, 082004.
- [27] K. Wu, P. Coquet, Q. J. Wang, P. Genevet, *Nat. Commun.* **2018**, *9*, 3494.
- [28] R. C. Devlin, M. Khorasaninejad, W. T. Chen, J. Oh, F. Capasso, *Proc. Natl. Acad. Sci. USA* **2016**, *113*, 10473.
- [29] J. A. Kurvits, M. Jiang, R. Zia, *J. Opt. Soc. Am. A* **2015**, *32*, 2082.
- [30] T. H. Taminiau, S. Karaveli, N. F. Van Hulst, R. Zia, *Nat. Commun.* **2012**, *3*, 979.
- [31] A. B. Vasista, H. Jog, T. Heilpern, M. E. Sykes, S. Tiwari, D. K. Sharma, S. K. Chaubey, G. P. Wiederrecht, S. K. Gray, G. V. P. Kumar, *Nano Lett.* **2018**, *18*, 650.